Ocean Color Imager: Instrument Description and Its Performance

L. S. Lee[1], K. Lo[1] and Y. J. Chiang[1]

ABSTRACT

The Ocean Color Imager is an electro-optic remote sensing instrument to be flown on the ROCSAT-1 satellite, scheduled to be launched in January 1999. It is a push-broom type spectral-radiometer with 702 km swath width and 800 m resolution for measuring radiances of water-leaving from ocean surfaces and atmospheric scattering in six visible and near infrared bands. The OCI's missions, architecture, function, and pre-launch performance test results are described here.

(Key words: Ocean Color Imager, ROCSAT-1, Remote sensing, Responsivity, Signal to noise ratio, Modulation transfer function, Anti-blooming)

1. INTRODUCTION

ROCSAT-1, the first satellite of the Republic of China on Taiwan, is scheduled to be launched in January 1999 (Figure 1). The main objective of this satellite program is to lay the foundation for local technical capabilities including satellite system development, ground system development and basic and applied research related to three scientific payload instruments. The Ocean Color Imager (Figure 2), or OCI, is one of the three payload instruments and is a spectral radiometer as well as a nadir looking push-broom imager for mapping the distribution of radiance from the ocean surface and atmospheric scattering in six visible and near infrared bands.

The Coast Zone Color Scanner (CZCS) on the Nimbus-7 satellite was the first space-borne instrument to acquire ocean color data, which became very useful for studying the role of ocean in the global carbon cycle and ocean circulation. The major characteristics and parameters of the CZCS, given in Table 1, led to massive production of high quality ocean imagery from the fall of 1978, until the summer of 1986, when the instrument ceased to operate. In August 1996, NASDA of Japan launched the Ocean Color and Temperature Scanner (OCTS) on the ADEOS satellite that had 12 spectral bands ranging from 412 nm to 12.5 μm and provided highly valuable data for research work in ocean optics. The ADEOS ceased to operate in June 1997, two months before the launch time of the SeaStar satellite. The Sea-

---

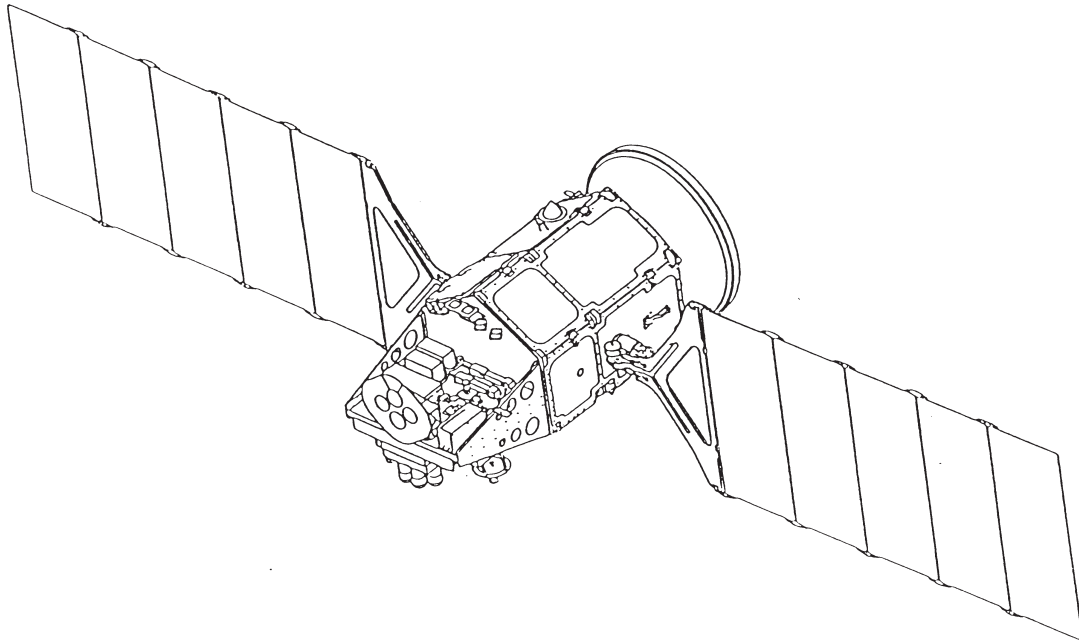[1]National Space Program Office, Hsin-Chu, Taiwan, ROC

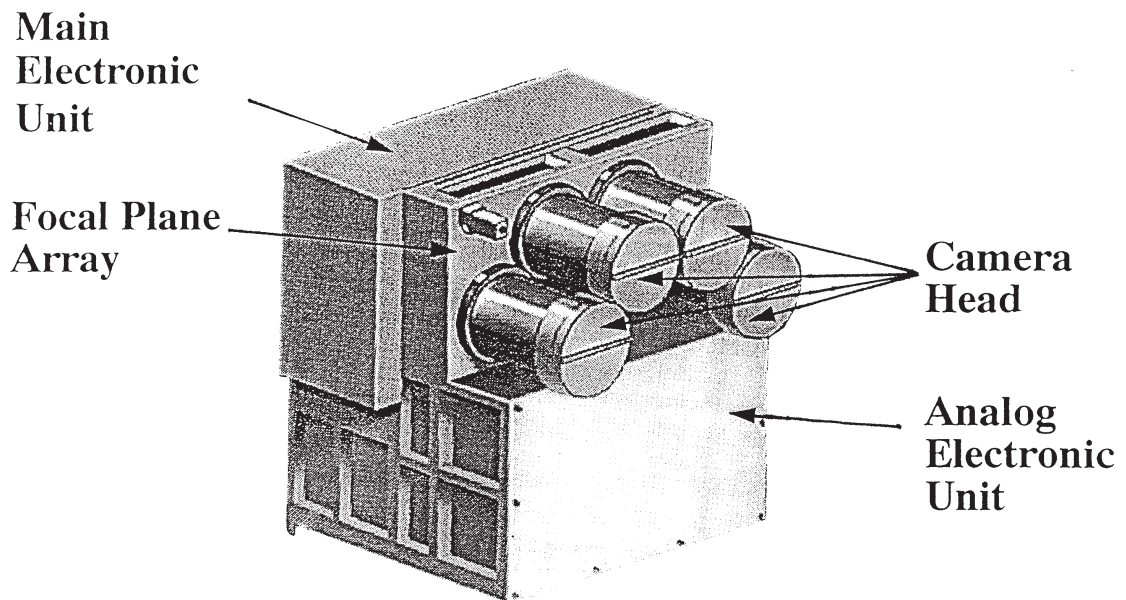*Fig.1*. Outlook of the ROCSAT-1 satellite.

Main Electronic Unit

Focal Plane Array

Camera Head

Analog Electronic Unit

Fig.2. Outlook of the OCI.

Table 1. The major characteristics and parameters of the CZCS.

Band number	1	2	3	4	5	6
Center wavelength	443 nm	515.nm	550 nm	670 nm	750 nm	11.5 μm
Mean radiance*	84.1	54.4	44.5	26.0	16.1	NA
Signal to noise ratio	350	342	280	209	50	NA
MTF @ Nyquist frequency	≥ 0.35	≥ 0.35	≥ 0.35	≥ 0.35	≥ 0.35	NA
Ground Resolution	825 meters					
Swath width	1600 km					
Orbit	Altitude = 955 km, sun synchronous					
Polarization	< 2 % sensitivity					
Radiance Accuracy	5 %, absolute.					

* Units of W/(Sr-m^2- μm)

viewing Wide Field-of-view Scanner (SeaWiFS) is a remote sensing instrument on the SeaStar satellite that has, since its launch time, obtained much valuable ocean optics data for assessing the ocean's role in the global carbon cycle, elucidating the magnitude and variability of the primary productivity by phytoplankton, and determining the distribution and timing of spring booms. The major characteristics and parameters of the SeaWiFS are given in Table 2.

The ROCSAT-1 program, including the OCI, is managed by the National Space Program Office (NSPO) of the Republic of China. The instrument is planned to take images normally between 9:00 AM and 3:00 PM local time with the imaging data processed by software developed by engineers and scientists at the Science Data Distribution Center (SDDC) in the National Taiwan Ocean University. Data results will be available to all the interested scientists doing research subjects in:

- mapping the pigment distribution in the low-latitude oceans and generating surface spectral data;
- studying marine productivity and the dynamics of meso-scale eddies; and
- investigating the influence of atmospheric aerosols in remote sensing.

Table 2. The major characteristics and parameters of the SeaWiFS.

Band number	1	2	3	4	5	6	7	8
Center wavelength (nm)	412	443	490	510	555	670	740	865
Mean radiance*	91.0	84.1	65.6	56.4	45.7	24.6	16.1	10.9
Signal to noise ratio	499	674	667	640	596	442	455	467
MTF @ Nyquist frequency	≥ 0.3	≥ 0.3	≥ 0.3	≥ 0.3	≥ 0.3	≥ 0.3	≥ 0.3	≥ 0.3
Ground Resolution	1100 meters							
Swath width	2800 km							
Orbit	Altitude = 705 km, sun synchronous							
Polarization	< 2 % sensitivity							
Radiance Accuracy	5 %, absolute.							

* Units of W/(Sr-m^2- μm)

A science team consisting of mainly local scientists will perform sensor calibration and atmospheric correction, and develop algorithms for validating the OCI data results concerning water-leaving radiance, pigment concentration, chlorophyll-a concentration, and ocean water attenuation coefficient.

2. ORBIT SELECTION

Unlike many low altitude earth observation satellites which are on sun-synchronous polar orbits, the ROCSAT-1 orbit is 600 km above the ground with 35° inclination angle. This orbit was selected in consideration of achieving the most contact time with the ground station in Taiwan and fulfilling the necessity of another payload, Ionospheric Plasma Electrodynamics Instrument (IPEI), to gain more operation time near the equator. The satellite orbit simulation results (Figure 3 and Figure 4) show that the orbit precession rate is ~ 6°/day and the satellite ground track repeat period is 52 days. By considering 702 km observation swath width and local observation time between 9:00 AM and 3:00 PM, the revisit time for a specific region, e.g. Taiwan, can be as short as one orbital period, ~97 minutes, or as long as 25 days.

3. BAND SELECTION FOR SCIENTIFIC OBSERVATIONS

Because of physical constraints and budget limitations, the OCI has six spectral bands that are similar to the SeaWiFS', but does not have the 412 nm and 865 nm bands. Table 3 shows the six selected bands, plus a redundant 555 nm band, their spectral characteristics, and corresponding scientific observations. The two bands with the longest wavelength, centered at 670 nm and 869 nm, are mainly for measuring atmospheric scattering. Since there is little reflectance from the ocean surface in these spectral regions, the measured data would be used for atmospheric correction. The measured data of the other four bands, centered at 444 nm, 492 nm, 512 nm, and 555 nm, are from atmospheric scattering and water leaving radiance. After correction, by subtracting the estimated radiance of atmospheric scattering, water leaving radiance values can be obtained and used to compute the pigment distribution near the ocean surface by using the validation and calibration algorithms developed by the science team.

B7 is a redundant of B4 for measuring greenish yellow radiance, which is nominally constant, i.e., independent of the chlorophyll concentration. The chlorophyll spectral radiance near 555 nm behaves like a "hinge" because the spectral radiance curves from different concentrations of chlorophyll "pivot" around this spectral position.

4. ARCHITECTURE

The OCI's hardware was built by the NEC Corporation and consists of three modules: the Optical Unit (OU), the Analog Electronic Unit (AEU), and the Main Electronic Unit (MEU). Its functional block diagram is shown in Figure 5.
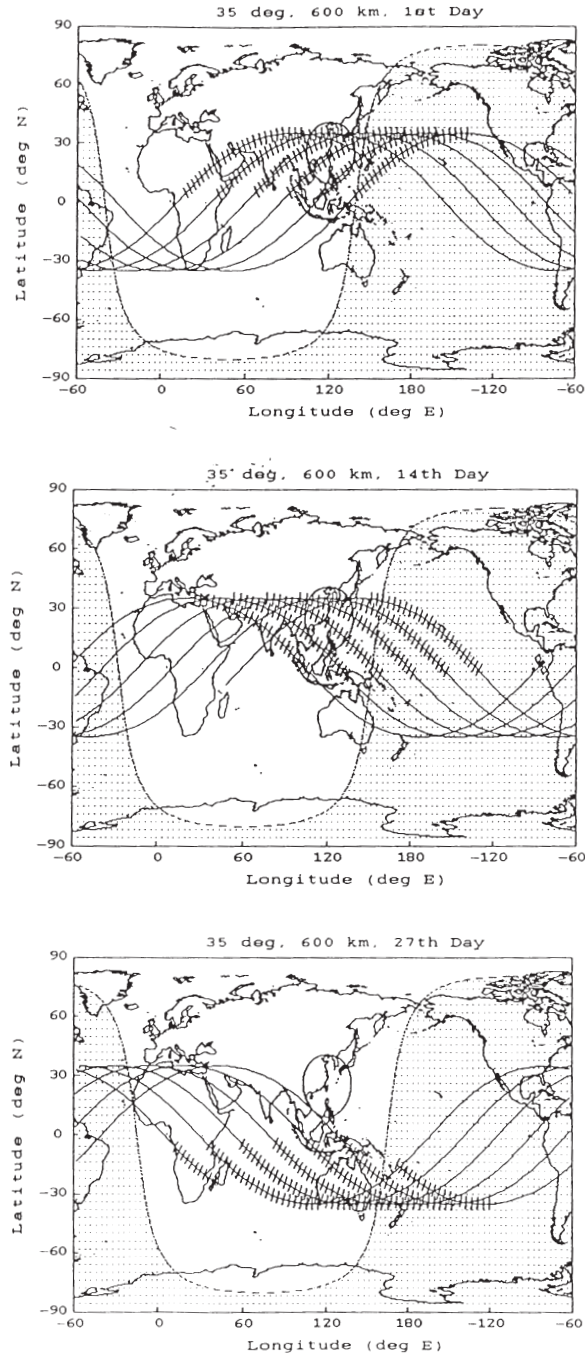
Fig.3. Computer simulation showing precession of the orbit with 35° inclina-
tion. Tick marks in the figure indicate the OCI observation coverage
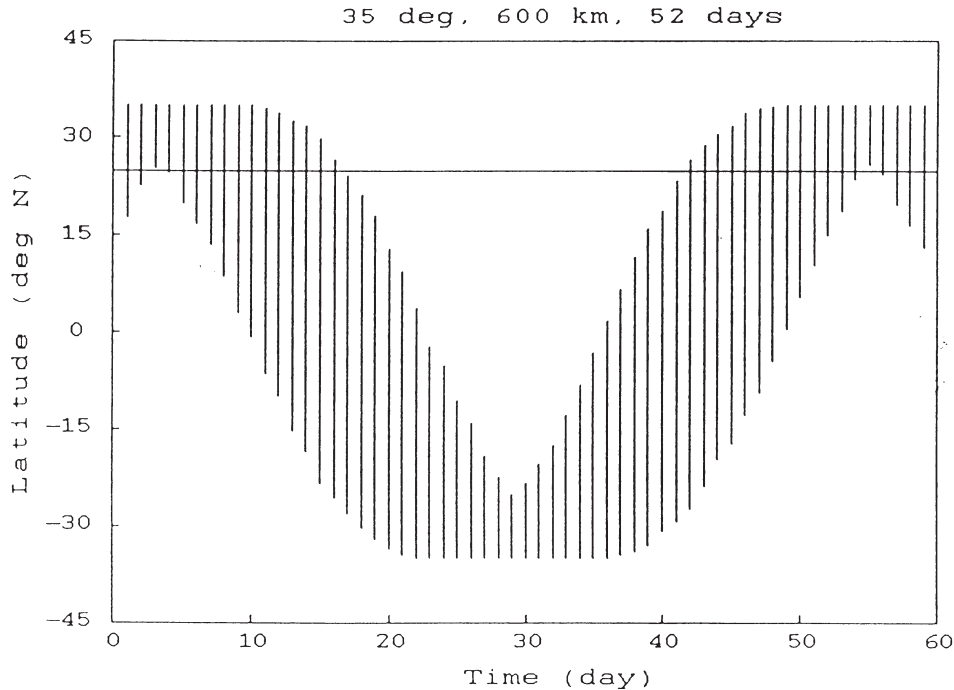between 9:00 – 15:00 local time.

Fig.4. Latitude variation of the OCI observation coverage due to the precession. Observation time is 9:00 - 15:00.

Table 3. The OCI band selection and scientific observation.

Band Number	Center Wavelength	Bandwidth, FWHM	Scientific Observations
B1	444 nm	20.0 nm	Chlorophyll Absorption
B2	492 nm	20.1 nm	Pigment
B3	512 nm	19.6 nm	Chlorophyll Absorption
B4	555 nm	18.5 nm	Hinge point, Sediments
B5	670 nm	18.5 nm	Atmospheric Scattering
B6	869 nm	40.3 nm	Atmospheric Scattering
B7	555 nm	18.5 nm	Same As That Of B4

The OU consists of four camera heads and seven linear array CCD devices (Thomson TH7811) for detecting radiances in seven spectral bands. Each camera head has an eight-lens telecentric telescope subsystem (Figure 6) with 19.5 mm focal length and 60.7° field of view (FOV) to give 702 km swath width at 600 km altitude. Two bands (B1/B3, B2/B4, or B5/B6) share a common lens subsystem in a camera head with a long back focal length. A phase plate that can scramble optical polarization is placed between the lens subsystem and a prism-type
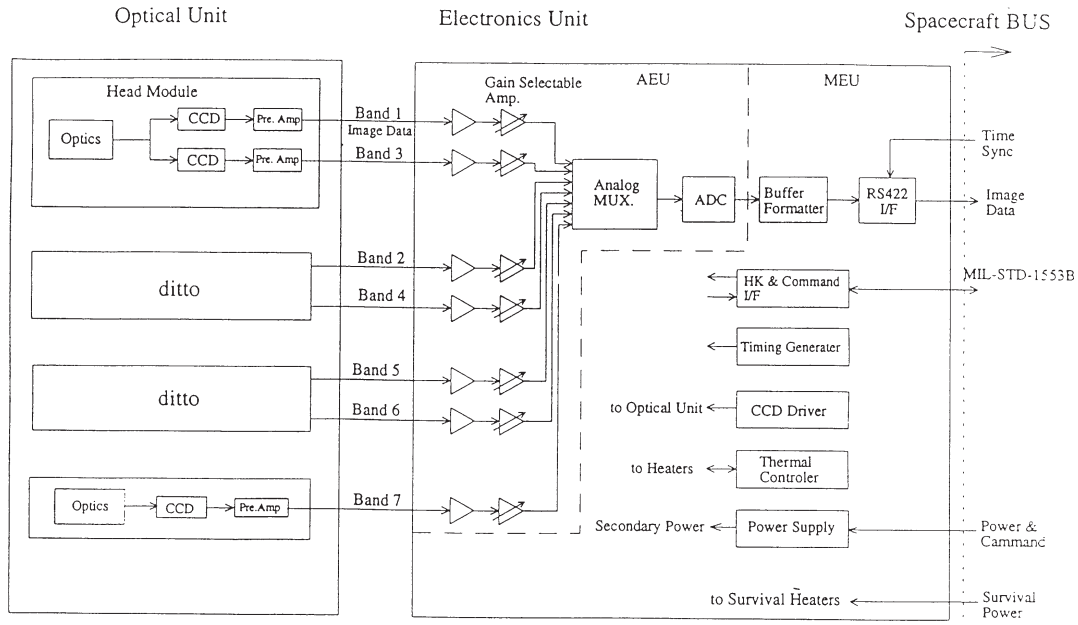
Fig.5. Functional block diagram of the OCI.

dichroic beam-splitter. The beam splitter is a long pass filter that can separate the light beam into two such that the transmitted (longer wavelength) and the reflected (shorter wavelength) ones will eventually form two images on two different focal planes. An interference type narrow band pass filter that largely determines the spectral bandwidth and center wavelength is placed in front of each CCD device. B7 uses a stand-alone camera head with a lens subsystem similar to that of the others. Because of the telecentric feature of each optical system, the light beams are incident normally on the interference filter and, over 60.7° FOV, the variation of center wavelength due to "blue-shift" effect in the filtering is insignificant.

The TH7811 linear CCD device has 1728 cells each with a $13 \mu m \times 13 \mu m$ photosite that can transform optical radiance into electric current. Since the OCI's data format allows each band to have 896 pixels, the cells in each device are arranged to give 64 single cell pixels in the center region of the array and 832 double cell pixels on both sides of the region. At 600 km altitude and with 19.5 mm focal length, 6.9 km/s ground track speed and 115.8 ms integration time, the nadir-looking push-broom mechanism will give $\sim 400m \times 800m$ ground resolution for the single cell pixel and $\sim 800m \times 800m$ ground resolution for the double cell pixel.

The CCD output signals are processed in the AEU to provide the desired gain and minimize the noise before multiplexing into a 12 bit A/D converter. The digitized signals are sent to and packetized according to CCSDS format in the MEU, which includes data format electronics, command and telemetry interface electronics, heater control electronics, and digital electronics power supply. The command signals and ancillary data, which include satellite attitude, position, timing, and instrument housekeeping, such as temperature, voltage and cur-

rent values are sent via a 1553B data bus. The image data are sent via an RS-422 data bus to the spacecraft where a solid state recorder with 2 Gbits memory capacity is used to store the OCI's image data, the IPEI's science data, and the housekeeping data of the three payloads and the spacecraft.

To avoid overloading the recorder's memory, the OCI's observation duty cycle will be ~ 3% for taking images, in one of the five observation modes (Table 4). The OCI will then be in the Standby mode, when not taking images.
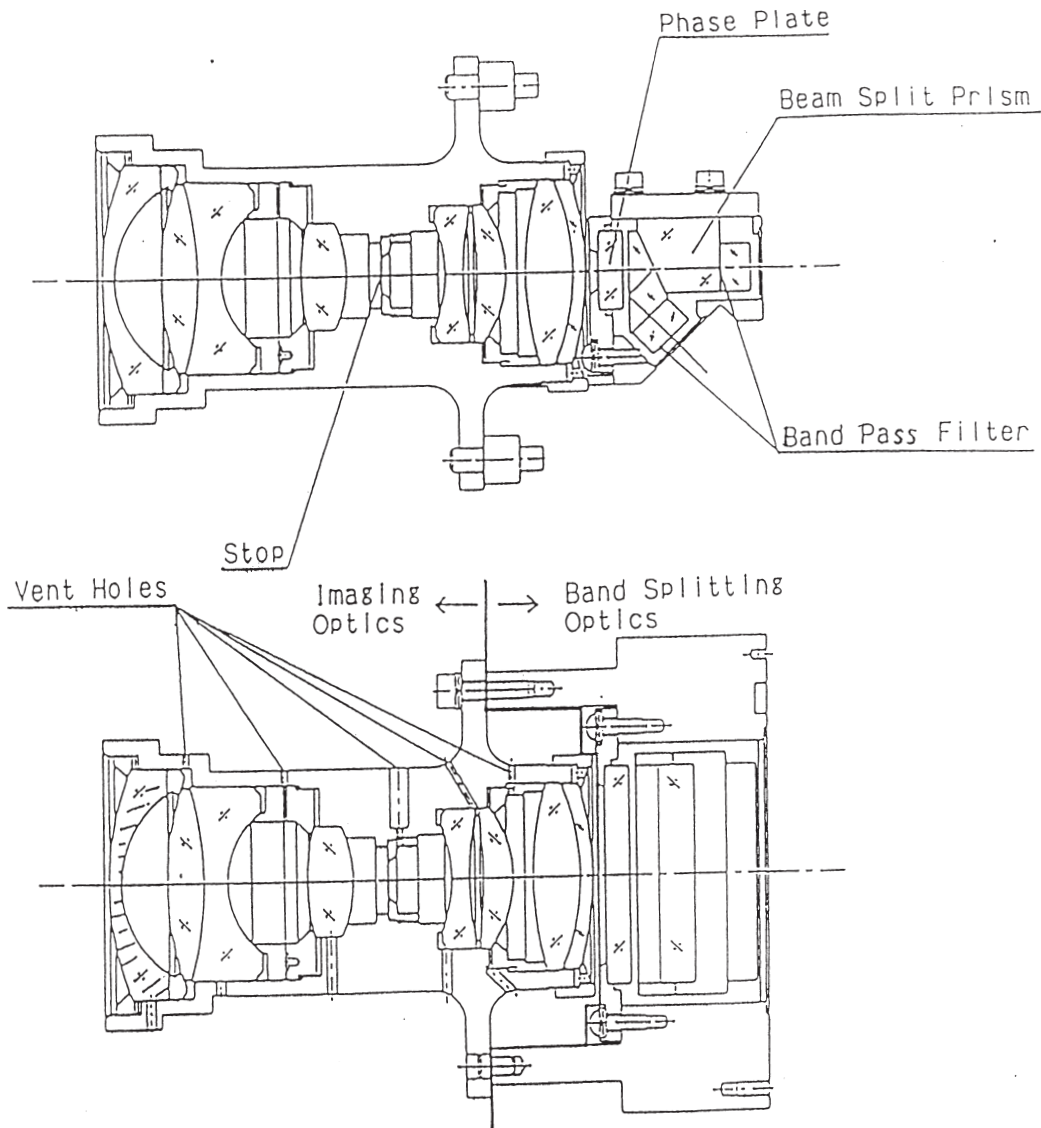

Fig.6. Side view and top view of a cut-away camera head.

Table 4. The OCI's observation modes and corresponding output bands.

Observation Mode	Output Imaging Data
Full Band Mode (FB)	B1, B2, B3, B4, B5, B6, and B7
Normal Imaging-A Mode (NI-A)	B1, B2, B3, B4, B5, and B6
Normal Imaging-B Mode (NI-B)	B1, B2, B3, B5, B6, and B7
RGB Mode (RGB)	B2, B4, and B6
Calibration Mode (CA)	B4 and B7

5. RESULTS OF PERFORMANCE TESTS

Before launch, the OCI underwent numerous functional, performance and environmental tests, including:

- initial instrument level functional and full performance tests;
- instrument level dynamic and thermal vacuum tests;
- instrument level EMI/EMC tests;
- final instrument level functional and full performance tests;
- initial satellite level functional tests;
- satellite level EMI/EMC tests;
- intermediate satellite level functional tests;
- satellite level dynamic and thermal vacuum tests; and
- final satellite level functional and selected performance tests.

The dynamic tests included sine and random vibration, acoustic and pyro-shock tests to verify that the sensor's function and performance would not degrade after going through an environment similar to that of the launch process. The thermal vacuum tests included hot balance, cold balance and 8 thermal cycles that simulated a satellite's orbital thermal condition in outer space. The EMI/EMC tests included electric and magnetic emission and conducted and radiated electric susceptibility tests. The functional tests included verification of electrical interface between the instrument and the spacecraft, or its simulator, such as command and telemetry signal transmission. The instrument level and satellite level tests were performed at the NEC site and the NSPO site, respectively. Instrument level full performance tests included: signal to noise ratio (SNR), modulation transfer function (MTF), spectral registration, anti-blooming, response linearity, dark signal, polarization sensitivity, and out of band spectral rejection, etc. Because of time and facility constraints, satellite level performance tests only included SNR and dark signal measurements. The results of all the performance tests were satisfactory, or better, and are described in the following sections.

5.1 Signal to Noise Ratio

To achieve good image quality, very high SNR values were specified for the sensor (Table 5). By using various approaches to minimize noise in the signal chain, very high SNR values,

>650 for double cell pixels, were finally achieved (Table 6). The approaches included:
- widening the telescope aperture to enhance the signal;
- controlling the CCD operation temperature at ~10°C to lower the thermal noise;
- using clamp and sample circuit to perform correlated double sampling;
- good shielding to block electro-magnetic interference as much as possible; and
- digitizing the signal into 12 bits to make the quantization noise insignificant.

The measurements were taken in an ambient environment at ~30°C by using a very stable 2 meter diameter integrating sphere with a 50 cm aperture and up to 26 well calibrated halogen lamps. It was further proven by simulation test in the thermal vacuum chamber that, in outer space, the CCDs temperature should be maintained at ~10°C, which should yield slightly higher SNR values due to lower thermal noise.

More measurement results taken at ~30°C also indicated that the SNR values would be higher than 300 even with relatively weak input radiance, ~1/5 of the corresponding mean radiance (Figure 7). Such good performance suggested that the sensor's observation time could be expanded from 9:00-15:00 to perhaps 7:30-16:30 local time.

5.2 Modulation Transfer Function

The MTF requirements for each band at Nyquist frequency are specified in Table 7.

Table 5. Specifications of signal to noise ratio.

Band Number	B1	B2	B3	B4	B5	B6	B7
Mean Radiance*	84.1	65.6	56.4	45.7	24.6	10.9	45.7
Required SNR for double cell pixels @ 10℃	≥ 450	≥ 450	≥ 450	≥ 450	≥ 350	≥ 350	≥ 450

* Units of W/(Sr-m^2-μm)

Table 6. The OCI's measured SNR values in the performance tests.

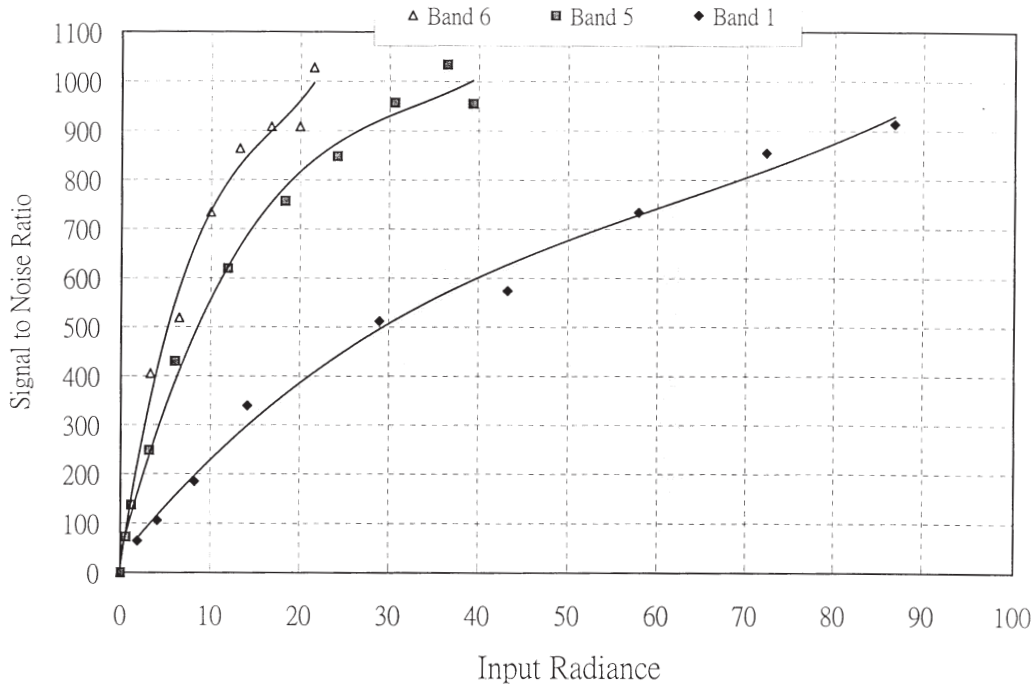| Band Number	B1	B2	B3	B4	B5	B6	B7
Input Radiance*	84.1	61.3	54.1	42.9	24.15	10.6	42.9
Measured SNR for double cell pixels @ 30℃	≥ 751	≥ 779	≥ 782	≥ 657	≥ 777	≥ 671	≥ 700
Measured SNR for single cell pixels @ 30℃	≥ 588	≥ 603	≥ 462	≥ 516	≥ 581	≥ 522	≥ 533

* radiance in W/(Sr-m^2-μm)

Fig.7. Examples of typical relation between SNR and input radiance. The data are from pixel #99, B6, B5, and B1. The results indicate that SNR decreases as input radiance weakens. However, SNR remains high (>300) even with 1/5 of the mean radiance, i.e., 2.2, 4.9, and 17 W/(Sr-m²- μ m) for B6, B5, and B1 respectively.

Table 7. Specification of MTF requirements for the bands.

Band Number	B1	B2	B3	B4	B5	B6	B7
Cross-track MTF	$\geq$0.30	$\geq$0.30	$\geq$0.30	$\geq$0.29	$\geq$0.24	$\geq$0.16	$\geq$0.29
Along-track MTF	$\geq$0.21	$\geq$0.21	$\geq$0.21	$\geq$0.20	$\geq$0.20	$\geq$0.19	$\geq$0.20

By selecting suitable optical glass materials for the eight lenses, each telescope subsystem was carefully designed to yield simulation results with static MTF better than 0.72 (Table 8). With unavoidable alignment errors, assembly errors, crosstalks, and simulated satellite motion effects, the instrument performance nevertheless showed good MTF measurement values, between 0.47 and 0.71 (Table 8).

After going through instrument level dynamic and thermal vacuum tests, the sensor showed little degradation in the MTF performance.

5.3 Band to Band Spectral Registration

With 60.7° FOV and 7 spectral bands ranging from blue to near infrared, making an opto-mechanical hardware with high accuracy in spectral registration among the bands is a great challenge. Tremendous efforts were made in optical design, component fabrication, alignment and assembly to minimize error sources such as mis-alignment and aberration. The registration accuracy requirements for the OCI hardware and the measured results in the performance tests are summarized in Table 9.

Some test results are shown in Figure 8. After going through instrument level dynamic and thermal vacuum tests, the instrument showed insignificant deterioration in the registration performance.

5.4 Anti-blooming

Anti-blooming is a CCD feature that can effectively reduce the charge spill over to their neighborhood when some CCD cells are illuminated by extremely bright incident light. When the OCI is used for observation, some objects such as clouds will look much brighter than the ocean. Consequently, the anti-blooming feature in CCD is desirable in order to avoid degradation of image quality attributed to the bright object smearing effect due to charge spill over phenomenon. By setting the saturation voltage at 6.5 V on TH7811 CCD chips, satisfactory anti-blooming performance as well as response linearity over the desired dynamic range both were achieved. The anti-blooming performance for each spectral band was measured by using

Table 8. The OCI's MTF values, by design and by test.

Band Number	B1	B2	B3	B4	B5	B6	B7
Static MTF by Optical Simulation	≥ 0.73	≥ 0.83	≥ 0.83	≥ 0.83	≥ 0.72	≥ 0.73	≥ 0.83
Measured Along-Track MTF	0.53	0.55	0.52	0.52	0.53	0.49	0.51
Measured Cross-Track MTF	0.68	0.66	0.71	0.58	0.62	0.47	0.68

Table 9. Specification and performance of the spectral registration.

	Along Track	Cross Track
Required Accuracy (with regard to the center of the 7-band distribution)	± 1.5 IFOV	± 1.43 IFOV
Test Results (with regard to the center of the 7-band distribution)	± 0.34 IFOV	± 0.62 IFOV

a bright stripe as the observation object with $20\times$ IFOV width and brightness that provided 6 times the saturation radiance. The results showed that blooming effects were limited to only $\leq 5\times$ IFOVs, or ≤ 10 CCD cells (Figure 9).

5.5 Spectral Responsivity

The relation between the instrument's output (digital counts) and its input (radiance) is attributed to the combined convolution of the subsystem/component response functions including, lens subsystem, dichroic prism, polarization scrambler, interference filter, CCD, analog electronics, and A/D conversion, etc. If the input radiance does not saturate the system, the relation will be:

$$\text{Output (of Nth Pixel)} = D_n + \int f(\lambda)\cdot \alpha_n \cdot P_n(\lambda)\cdot G\cdot L(\lambda)d\lambda \qquad (1)$$

where,

D_n is dark signal of Nth CCD pixel and is wavelength independent;

$f(\lambda)$ is the combined paraxial spectral transmission of the lens subsystem, dichroic prism,
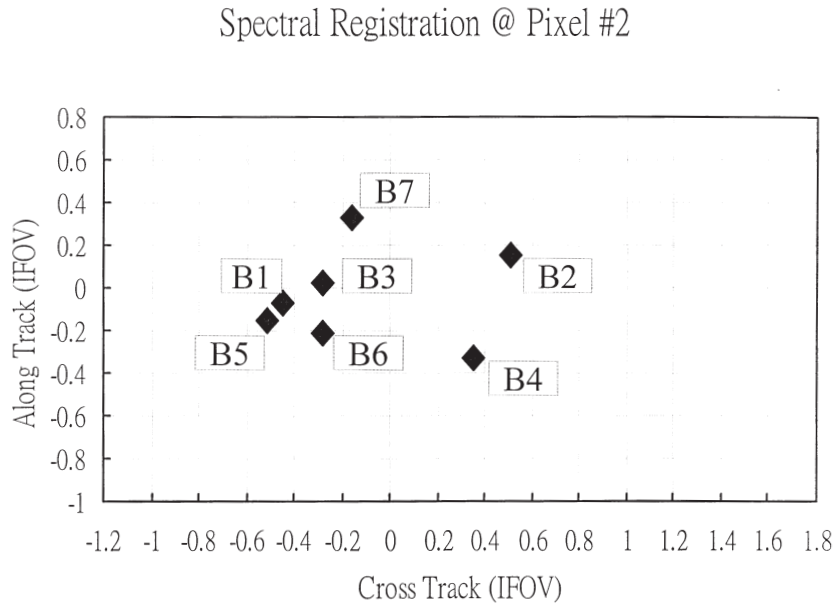
Fig.8. An example of spectral registration measurement result. The data are from pixel #2, which is located near FOV edge, a position very difficult to perform good alignment, especially in the along track direction. The result indicates that, at this position, the registration distribution is within ± 0.34 IFOV, along track, and ± 0.52 IFOV, cross-track. IFOV stands for instantaneous field of view. One IFOV for the OCI is equivalent to 800 meter ground sampling distance.

polarization scrambler, and interference filter;

α_n is the off-axis optical attenuation factor that is responsible for signal non-uniformity over the FOV (Figure 10) and is wavelength independent;

$P_n(\lambda)$ is the spectral responsivity of the Nth pixel;

G is the factor of circuit gain and A/D conversion and is wavelength independent; and

$L(\lambda)$ is the OCI's input radiance.

By using available values of f, α_n, P_n and G we have computed their products to get $F_n(\lambda)$ for each pixel in each band, which can be used to predict the instrument's output when the input radiance is known, (Figure 11) i.e.,
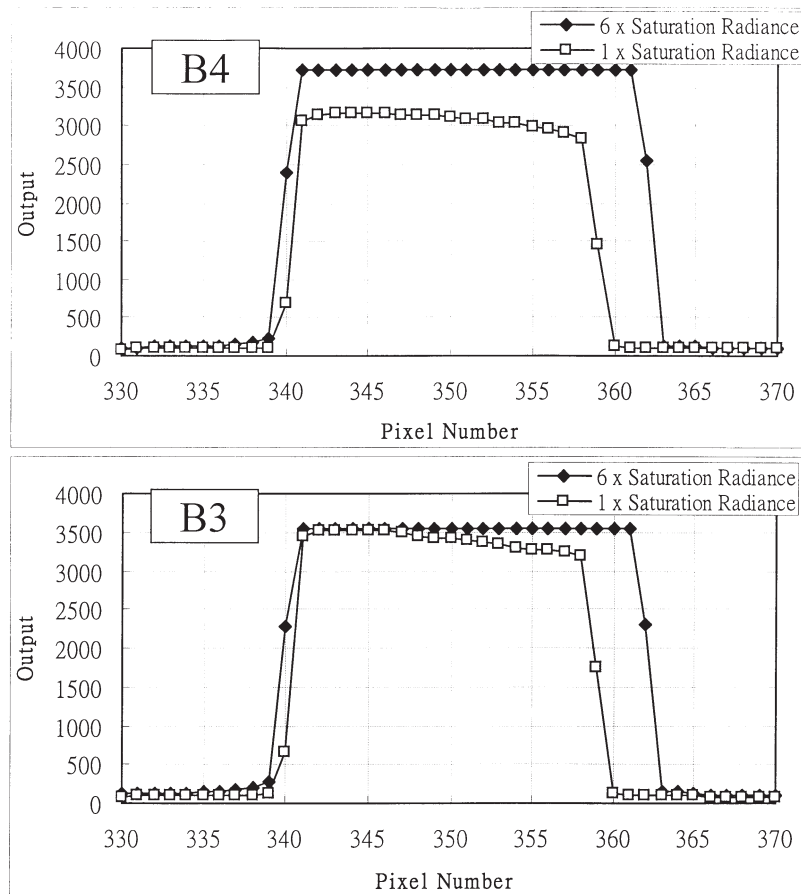
Fig.9. Two examples of typical anti-blooming measurement results (B3 & B4). A bright stripe that generated 1× the saturation radiance was first used as the observation object for the measurement. The brightness of the stripe was later increased to provide 6× the saturation radiance and the measured results showed that the blooming effect was within 2 pixels on one side and within 5 pixels on the other side.

$$\text{Output (of Nth Pixel)} = D_n + \int F_n(\lambda) \cdot L(\lambda) d\lambda \tag{2}$$

Since the band-shape of $F_n(\lambda)$ is very narrow, we can assume that $L(\lambda)$ is nominally constant within the band and we can simplify Equation **2** to:

$$\text{Output (of Nth Pixel)} = D_n + \phi_n(\lambda_c) \cdot L(\lambda_c) \tag{3}$$

where,

λ_c is the center wavelength, as shown in Table 3 and

ϕ_n is the average responsivity.

5.6 Response Linearity

The saturation radiance values (Table 10) specified for the OCI's spectral bands are identical to that for the SeaWiFS. The performance test results at ~30°C showed fairly good, or better, linearity for every band within the specified radiance range. The light source for testing radiometric responsivity was the same as that for testing SNR. In order to vary the light source output radiance over the desired range, from 0, 3.3, 6.5, ..., to 132 W/(Sr-m²-μ m), the number of lamps turned on was varied from 0, 2, ..., to 26 in the integrating sphere, as the lamp voltage was adjusted from 25.8 to 90.0 volts. The results indicated a little saturation effect for all the bands except for B4, which had the best response linearity and was without saturation. The linearity was so good that the relation between the output signals, in digital counts, and the input radiance of B4 could be approximated by a first order polynomial with little discrepancy, largely determined by the noise amplitude (Table 11).

However, if first order polynomials were used to approximate the output/input dependence for the other bands, the discrepancy could be as large as ~1 %, or five times the noise amplitudes, due the nonlinear feature of the saturation effect. If third order polynomials were used as the fitting curves, the matching discrepancies would become much smaller, as large as the noise level (Table 12).
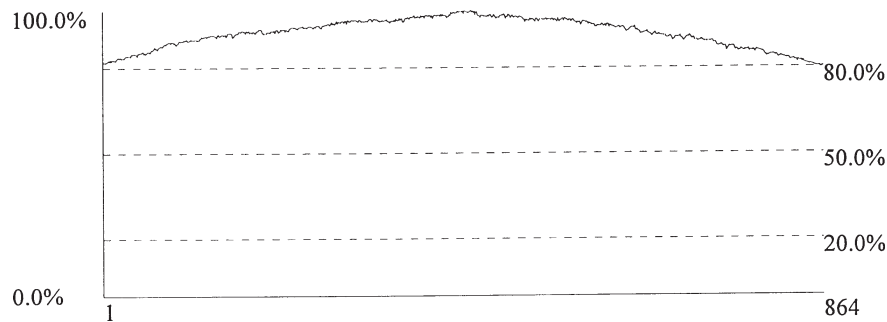
Fig.10. An example of measurement results on response non-uniformity (B1). The response at the edge is minus 21% with regard to the max. near the center. The performance is significantly better than the requirement specified in Table 13.
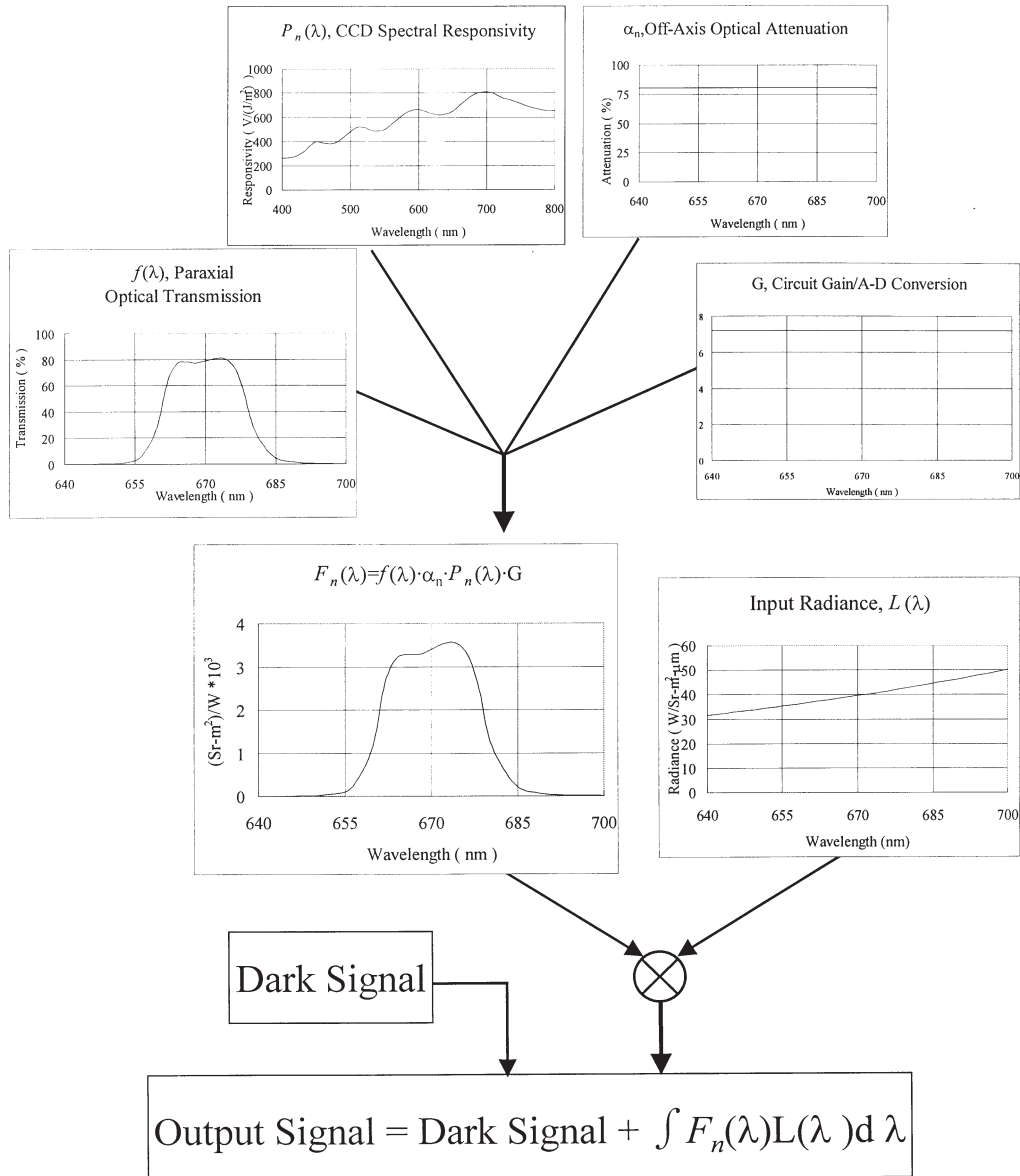
Fig.11. Derivation of the OCI output from its input (radiance). Negligible saturation effect is assumed. $F_n(\lambda)$ data are from pixel #1, B5. The unit of horizontal axes is nm.

5.7 Dark Signal vs. Temperature

In Table 11 and Table 12 the signals were greater than zero even when the radiance values were zero. Dark signals of this kind were attributed to circuit offsets and thermal agitation in

the CCD cells as well as noises from the CCD cells, analog electronics and A/D conversion. The dark signals were temperature dependent, and could vary from band to band as well as from pixel to pixel. We have analyzed numerous dark signal data and found that the signal value could be estimated by:

$$\text{Dark Signal (in digital count)} = \text{Circuit Offset} + R_n \cdot 2^{T/Q} \qquad (4)$$

where,

"Circuit Offset" = 34.3 ± 2.6, had different values for different CCD chips;

"R_n" = 7.1 ± 1.6, varied from pixel to pixel;

"Q" = 8.9 ± 1.2°C, varied from chip to chip; and

"T" was the CCD temperature in °C.

5.8 Measurement Results on Selectable Gains

The OCI's functional block diagram shows that, for each band, there is a gain selector designed to provide normal gain =1.0, low gain =0.5, and high gain =6.0 for B7 and =2.0 for

Table 10. Specification of saturation radiance for the bands.

Band Number	B1	B2	B3	B4	B5	B6	B7
Saturation Radiance W/(Sr-m^2-μm)	132.5	105	90.8	74.4	42	21.3	74.4

Table 11. An example of response linearity. (data from pixel #486, B4.)

Input Radiance W/(Sr-m^2-μm)	0	10.43	21.48	31.97	42.87	53.53	64.35	69.75
Output — By measurement at ~30°C (in digital counts)	95.8	459.9	850.4	1222.6	1610.0	1986.4	2360.9	2548.5
Output — By approximation with a first order polynomial*	95.3	462.7	852.0	1221.6	1605.6	1981.2	2362.3	2552.6

* $Y = 35.23 \cdot L + 95.29$

Table 12. An example of response (non)linearity. (data from pixel #486, B2.)

Input Radiance W/(Sr-m^2-μm)	0	14.98	30.73	45.78	61.28	76.56	91.92	99.51
Output — By measurement at ~30°C (in digital counts)	92.0	592.6	1128.6	1640.0	2165.8	2667.2	3155.0	3394.6
Output — By approximation with a first order polynomial*	103.3	602.1	1126.5	1627.6	2143.7	2652.4	3163.8	3416.3
Output — By approximation with a third order polynomial$^+$	91.4	593.6	1128.6	1640.8	2163.5	2668.2	3159.0	3393.6

* $Y = 33.295 \cdot L + 103.34$ $^+ Y = -0.00027 \cdot L^3 + 0.02694 \cdot L^2 + 33.177 \cdot L + 91.427$

the other bands. The measurement results show that the actual ratios among gain values for different bands were:

$$0.4974_{(\pm 0.0009)} : 1 : 1.996_{(\pm 0.007)} \quad \text{for B1;}$$
$$0.4993_{(\pm 0.0011)} : 1 : 2.002_{(\pm 0.006)} \quad \text{for B2;}$$
$$0.4994_{(\pm 0.0009)} : 1 : 1.9995_{(\pm 0.004)} \quad \text{for B3;}$$
$$0.4997_{(\pm 0.0011)} : 1 : 2.002_{(\pm 0.004)} \quad \text{for B4;}$$
$$0.4995_{(\pm 0.0011)} : 1 : 2.001_{(\pm 0.004)} \quad \text{for B5;}$$
$$0.4994_{(\pm 0.0011)} : 1 : 2.004_{(\pm 0.006)} \quad \text{for B6; and}$$
$$0.4997_{(\pm 0.0011)} : 1 : 5.998_{(\pm 0.009)} \quad \text{for B7.}$$

5.9 Other Performance Requirements and Measurement Results

The requirements and the measurement results of signal uniformity, out-of-band spectral rejection, radiometric accuracy, polarization sensitivity, mass, size and power consumption are summarized in Table 13.

Table 13. Other OCI system requirements and measurement results.

Specification Item	Requirements	Measurement Results
Signal Uniformity	+0/-35%	+0/-21% (Figure 10)
Radiometric Accuracy	$\leqq$5%, absolute	3.8%, absolute
Polarization Sensitivity	$\leqq$2% (goal)	$\leqq$2%
Mass	$\leqq$16.8 kg	15.2 kg
Size	$\leqq$38cm x 35cm x 34.5cm	37.9cm x 34.9cm x 34.2cm
Power Consumption	$\leqq$33W peak, $\leqq$18W Standby	33W peak, 17.4W Standby
Out of Band Spectral Rejection	$\leqq$0.4%	$\leqq$0.22%

6. CONCLUSION

A spectral radiometer without any moving parts has been built and tested. It is a nadir-looking push-bloom ocean imager with good performance. Its weight is 15.2 kg and volume is 45.3 liters and, with 60.7° FOV and 0.077°IFOV (@ nadir), its swath width is 702 km and ground resolution is 800 meters at 600 km altitude. The results of performance tests suggest that, with very high SNR, MTF, and anti-blooming efficiency, the sensor's image quality would be very good. Since high SNR values are achievable with weak input radiance, the instrument's observation time could be expanded from 9:00-15:00 to perhaps 7:30-16:30 local time.

and monitoring the instrument design and fabrication, and NEC engineers, for their outstanding efforts in building and testing this fine performance sensor and its ground support equipment under a very tight schedule. Our science team, under the leadership of Dr. H-W Li and Dr. C-T Liu, have provided us much valuable and useful advise. This program has been supported by the National Science Council of the Republic of China.

REFERENCES

Gordon, Howard R., 1998: In-orbit Calibration Strategy for Ocean Color Sensors. *Remote Sensing and Environment*, **63**, 265-278.

Hooker, S. B., W. E. Esaias, G. C. Feldman, W. W. Gregg and C. R. McClain. 1992: SeaWiFS technical report series volume 1, An Overview of SeaWiFS and Ocean Color. Technical Memorandum 104566, 1, NASA, Greenbelt, MD.

Lin, W-S, J-Y Wu, H-J Chiu, C-S Chen and Y-J Chang, 1999: Sensor Calibration of the Ocean Color Imager. *TAO*, supplementary issue, March, 63-84.

McClain, C. R., W. E. Esaias, W. Barnes, B. Guenther, D. Endres, S. B. Hooker, B. G. Mitchell and. R. Barnes, 1992: SeaWiFS technical report series volume 3, SeaWiFS Calibration and Validation Plan. Technical Memorandum 104566, **3**, NASA, Greenbelt, MD.

Narimatsu, Y. et al., 1997: Ocean Color Imager Instrument: Critical Design Review. NEC Space System Division. OCI-BS-244-NEC.

Narimatsu, Y. et al., 1997: ROCSAT-1 Program: Ocean Color Imager FM Delivery Data Package. NEC Space System Division. OCI-BS-037-NEC.

Yang, B. T., 1995: The First Ocean Remote Sensing Payload of the ROC: An introduction. Oceanic Microwave Remote Sensing Workshop. COSPAR colloquium: Remote Sensing of Subtropical Oceans, NSC, 13A2-1.